Open Ceramics 3 (2020) 100020

Contents lists available at ScienceDirect

Open Ceramics

journal homepage: www.editorialmanager.com/oceram

Defect detection in additively manufactured lattices

J. Wilbig [a,*], F. Borges de Oliveira [b], A.-F. Obaton [c], M. Schwentenwein [d], K. Rübner [a], J. Günster [a]

[a] Bundesanstalt für Materialforschung und Prüfung, Unter Den Eichen 44-46, 12203, Berlin, Germany
[b] Physikalisch-Technische Bundesanstalt, Bundesallee 100, 38116, Braunschweig, Germany
[c] Laboratoire National de Métrologie et d'Essais, 1 Rue Gaston Boissier, 75015, Paris, France
[d] Lithoz GmbH, Mollardgasse 85a/2/64-69, 1060, Vienna, Austria

ARTICLE INFO

Keywords:
Additive manufacturing
Quality assurance
Defect detection
Lattices
Scaffolds
Ceramics

ABSTRACT

This paper investigates fast and inexpensive measurement methods for defect detection in parts produced by Additive Manufacturing (AM) with special focus on lattice parts made of ceramics. By Lithography-based Ceramic Manufacturing, parts were built both without defects and with typical defects intentionally introduced. These defects were investigated and confirmed by industrial X-ray Computed Tomography. Alternative inexpensive methods were applied afterwards on the parts such as weighing, volume determination by Archimedes method and gas permeability measurement. The results showed, that defects resulting in around 20% of change in volume and mass could be separated from parts free of defects by determination of mass or volume. Minor defects were not detectable as they were in the range of process-related fluctuations. Permeability measurement did not allow to safely identify parts with defects. The measurement methods investigated can be easily integrated in AM process chains to support quality control.

1. Introduction

Additive Manufacturing (AM) is an emerging technology, which enables the manufacturing of products easily tailored to individual needs. With this advantage, AM is of interest for several branches of industry – such as the medical device industry. The creation of anatomically matched devices and surgical instruments (e g. guides) is facilitated and complex geometric structures like twisted inner channels or specifically designed porous structures (lattices) can be easily realized. But a lack of experience and clinical history concerning the layer-wise manufacturing method presents currently a drawback in the acceptance of this technology. Quality assurance methods are needed to increase confidence in additively manufactured parts. [1]

Focus thereby is on non-destructive measurement methods, which ideally need to be fast to perform, inexpensive and easy to integrate into the manufacturing chain. Currently, a powerful tool to qualify a medical device is industrial X-ray Computed Tomography (XCT), which allows to check not only for dimensional errors compared to the nominal model but also for internal defects. Drawback on the other hand is the time consuming and expensive nature of the method, which makes it suitable for the characterization of prototypes during development or also for First Article Inspection (FAI), but not necessarily for routine measurement during mass production. Therefore, alternative measurement methods need to be investigated regarding their suitability to detect certain typical kinds of defects occurring in additively manufactured parts. [1]

Within the European project called MetAMMI – Metrology for Additively Manufactured Medical Implants [1], several measurement methods have been investigated on parts produced by different AM technologies and different materials. This article will present some of the measurements performed on lattice specimens, thereby focusing on parts produced by Lithography-based Ceramic Manufacturing (LCM) made of Tricalcium phosphate (TCP). A possible medical application for a lattice structure made of such bioceramics can be found in the field bone of substitution. Taking full advantage of AM for medical products, requires full process control and reliable methods for defect detection along the entire process chain.

The methods investigated are mass measurements of the printed part in order to identify defects by variations in the mass and also the detection of defects by variations in the volume of the manufactured lattice objects, using the Archimedes method. Another approach is to investigate the permeability coefficient of the parts by gas permeability measurement, which is expected to show defects in lattice parts by variation in the gas flow, that is applied through the part.

* Corresponding author.
E-mail address: janka.wilbig@bam.de (J. Wilbig).

https://doi.org/10.1016/j.oceram.2020.100020
Received 12 May 2020; Received in revised form 15 July 2020; Accepted 20 August 2020
Available online 28 August 2020

Lattice parts without and with defects were produced with LCM. Typical defects occurring in LCM production of lattice specimens, for example clogged cells or channels or overall thicker struts, were artificially introduced. These kinds of defects are also transferable to other AM technologies, as closed cells for instance represent also a common challenge in powder-based AM technologies. Suitable measurement methods identified on parts produced by LCM can be useful for quality control in AM in general.

To confirm the intentionally introduced defects, the printed parts without and with defects have been characterized by XCT. Subsequently, the parts have been characterized with the methods proposed regarding their properties such as mass, volume and permeability.

2. Lithography-based ceramic manufacturing (LCM)

LCM technology is based on the vat photopolymerization principle (as defined in ISO/ASTM 52900) and enables the layer-wise manufacturing of ceramic parts featuring material properties comparable to conventionally manufactured high performance ceramic parts [2].

Fig. 1 shows the CeraFab 7500 system, which was used to print the samples investigated in this work, as well as its basic components. The build process occurs bottom-up, when the build plate (1) is moved to a vat leaving a gap corresponding to layer thickness. On the rotating material vat (2) a layer of ceramic suspension is applied via a blade. The suspension consists of solid ceramic particles well dispersed in a liquid photopolymerizable resin, which can be selectively cured by the irradiation with light. Individual mirrors of a digital mirror device (3) can be selectively turned on and off illuminating/exposing the entire area of each cross section of the 3D object at once and thus curing the resin in defined areas of the individual layers by photopolymerization. LED light is used for curing (4). Afterwards, the solidified layer which is attached to the build plate is separated from the material vat by tilting it away from the build plate. The layer is finished and the sequence repeats, to finally produce the so-called green part, which is a composite of ceramic particles in a polymer matrix. The green part is finally removed from the building platform and immediately cleaned from any remaining suspension which may adhere to its surface. The cleaning is performed by pressurized air to remove excessive suspension followed by treating the parts with a cleaning solvent (LithaSol 30). The parts are placed in the cleaning solvent for 10 s and again treated with pressurized air. This procedure is repeated twice. Then, to obtain dense ceramic parts, the polymer is removed from the green part by thermal decomposition. Subsequent high temperature treatment up to 1200 °C leads to densification of the 3D object by sintering of the ceramic particles, which is β -TCP (LithaBone TCP 300) in this case. [2,3]

Fig. 2. Lattice with Wurtzite type structure (H: 8.5 mm; D: 6.8 mm).

The resulting ceramic parts typically show high densities (relative density of 98.0% for LithaBone TCP 300 [4]), a smooth surface and homogeneous microstructure. Due to the sinter process shrinkage of the part occurs. This shrinkage is specific for each ceramic suspension and thus can be automatically compensated by the printer software.

3. Designed defects

To evaluate the suitability of the different measurement methods to identify typical defects in the printed parts, a Wurtzite type structure as shown in Fig. 2 has been designed with nominal height, diameter and a strut thickness of 8.5 mm, 6.8 mm and 0.5 mm, respectively. The same

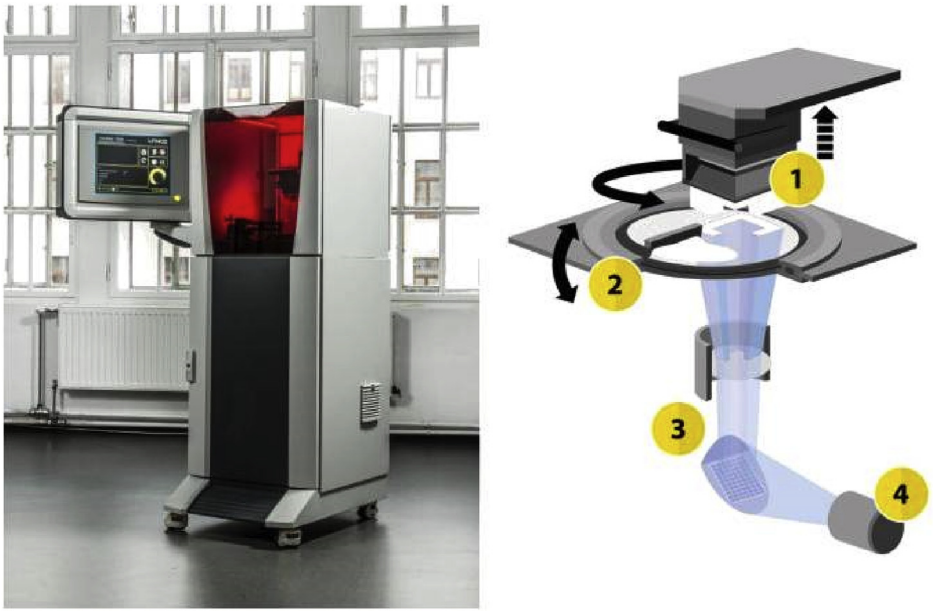

Fig. 1. CeraFab 7500 and fabrication unit.

structure was modified, and four kinds of defects were intentionally introduced. For processing in the LCM equipment, the 3D models were converted from CAD (Computer-aided design) to STL (Standard Triangulation/Tesselation Language) file format.

A typical defect in such filigree parts, when produced by AM is for example closed cells due to remaining material, which is not completely removed during the cleaning step. This is resin in case of the LCM technology (and similarly for other vat photopolymerization AM technologies) but could also be residual powder in parts produced by powder-based AM technologies. The second type of defect investigated was the final strut thickness exceeding the one designed in the 3D model. This defect is particularly relevant in the case of LCM, because it can be a result of over-polymerization. An analogue type of defect is the final strut thickness overall being thinner compared to the 3D model, which could influence the mechanical stability in service. The last type of defect investigated in this study is missing features, which can occur during handling of these delicate parts.

Fig. 3 shows the top view on the lattice designs, also referred to as scaffolds, with intended defects. The part without defects is presented in Fig. 3a compared to 20% thicker struts in 3b, 20% thinner struts in 3c, two completely filled cells and one membrane in 3d and missing struts in 3e.

Table 1 summarizes the nominal volume of the parts without and with defects in mm^3, determined from both CAD and STL files by integrating the filled volume elements. A change in the volume of the parts of about 2% can be observed after file conversion from CAD to STL, which is probably related to the resolution of the triangulation. In addition, the volume of the filled cells and missing struts are under and over interpreted respectively as a result of the conversion process. In the following, the STL data will serve as basis for the comparison between virtual model and printed part. The volume variation of the parts with defects compared to the reference volume of the scaffold without defects, which represents 100%, is listed in Table 1 as well as the designed porosity of the different scaffolds. By the ratio of the volume of the free space and the volume of an ideally full cylinder of the same outer dimensions, which is 308.7 mm^3 for this geometry, the designed macro porosities can be calculated. The scaffold shown in Fig. 3e has in total three missing struts, leading to a change in volume of 1.2% compared to the total volume of the part without defects. Diameter and height are the same for all parts and are not influenced by thicker and thinner struts.

As shrinkage of the parts during the necessary sinter step in the production process is typical, the STL files of the parts were scaled up for manufacturing to compensate for sintering shrinkage and to finally reach the desired dimensions. A scaling factor of 1.257 has been used in x-y-directions and of 1.292 in z-direction (height of the cylinder). With a layer thickness of 25 μm, the parts were printed from β-TCP. In total 30 parts have been printed (10 without defects and 5 parts per defect type) and analysed as described in the following.

4. Verification of designed defects by XCT

One part per defect type and one part without defects were scanned by XCT (Nikon MCT225, 160 kV, 50 μA, 7.6 μm voxel size), thereby the intended defects in the parts have been verified as presented in Fig. 4. Besides intended defects, further defects such as delamination defects (visible in Fig. 4b), missing materials (visible in Fig. 4c) and extra material could be identified as well.

Table 1
CAD volume and STL volume with percentage variation and designed porosities of parts with and without defects.

Defect type	**Without** (a)	**Thicker struts** (b)	**Thinner struts** (c)	**Filled cells** (d)	**Missing struts** (e)
CAD Volume [mm^3]	99.0	128.7	69.9	100.6	98.7
STL Volume [mm^3]	97.8	126.4	67.9	98.5	96.6
STL Volume variation [%]	reference	+29.2	−30.6	+0.7	−1.2
Designed porosity [%]	68	59	78	68	69

Quantitative analyses were also carried out in the XCT measurements of the parts. The overall volume, porosity, outer geometry, overall geometry deviation and strut thicknesses (of inner struts) were determined. The overall volume was calculated based on the XCT volumetric pixels (i.e. voxels). The algorithm counts the number of voxels present within the object and from that calculates the total volume. Advanced algorithms for XCT allow sub-voxels precision for this kind of measurements. For the porosity measurements, an algorithm implemented in the commercial software for XCT visualisation and measurement VG Studio Max 3.0, Heidelberg, Germany was used. The algorithm searches for pores within a determined by the user range of pore size and provides the percentage of the pores relative to the total volume. The outer geometry was determined by a scaling factor based on the outer contour of the scaffolds, i.e. measurement of the outer diameter and the height, and comparison with the nominal model (i.e. STL model). The overall geometry (inner and outer) was evaluated by an actual/nominal comparison of the measured/produced part with the nominal STL model of all parts. The deviation distribution of each measured part was determined. Absolute deviations in μm at 50% and 90% of the total deviation are used as metrics to characterise the AM parts. The strut thickness was calculated based on geometrical measurements (of cylinders) in the struts. Diameters of the cylindrically shaped struts were measured in different regions of the scaffold and the averaged diameter is presented in Table 2.

Table 2 summarizes the results of quantitative analyses. When considering the volumes obtained by XCT and assume the part without defect being 100%, the real variations in volume between the different defects are +20.9% with thicker struts, −23.3% with thinner struts, +2.6% with filled cells and +3.5% with missing struts. They differ from expected values described in Table 1. Although it is expected that the part with missing struts would feature a smaller volume compared to the reference, in fact a bigger volume was calculated. This difference from the expected results can be explained by the strut thickness results, which for the part with missing struts was slightly bigger than the part without defects. Besides this, extra material and delamination was observed in the part with missing struts (see Fig. 5), which can also explain the larger volume than the part without defects.

From total defect volume determined and porosity calculated, the

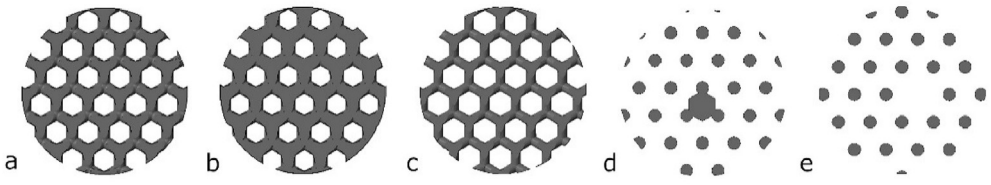

Fig. 3. Scaffold without defects (a) compared to scaffolds with intended defects, that are thicker struts (b), thinner struts (c), filled cells (d) and missing struts (e) (one representative slice of the STL file is shown for each designed object).

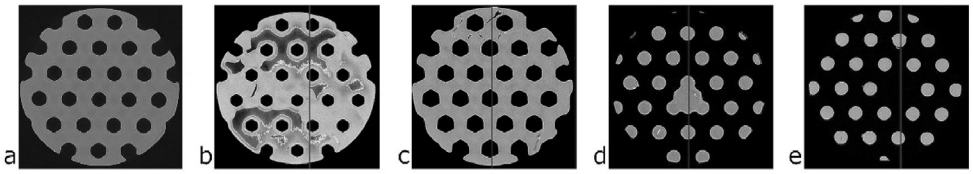

Fig. 4. XCT images of scaffolds without designed defects (a) compared to scaffolds with intended defects, that are, thicker struts (b), thinner struts (c), filled cells (d) and missing struts (e) (the images are reconstructions of XCT scan data of a representative layer in the xy-plane of the part).

parts appear to be nearly dense. The scaling factor of XCT data to the size of the STL file allows to quantify the dimensional variation of the outer geometry between measured part and STL file. In all cases the measured part was in all directions slightly bigger than designed - apart from the parts without defects, typically more in z-than in x-y-direction. Generally, the variation of the outer geometry is lower than 2%, while the absolute values for the overall geometry deviation are between 110 and 165 µm (at 90% of total deviation). The struts are in all cases on average (94 ± 6) µm thicker than designed.

In order to confirm the XCT measurements, the samples were scanned again with a second XCT system. A MicroCT 40 system from SCANCO Medical was used at 70 kV, 57 µA with a voxel size of 8 µm. The volume of the parts was determined with VG Studio Max 3.2 and is visualized for comparison in Fig. 8.

5. Defect detection by weighing

A measurement of the final parts mass by weighing is arguably the simplest approach to identify the different defects introduced, compared to the reference part without defects. With the nominal volume known from the STL file and the density of the solid material used for manufacturing, the final expected mass of the part produced can be calculated. In the following, the expected calculated masses are presented for the different geometries as well as a comparison to the masses determined.

Table 2
Results of quantitative analyses in XCT measurements.

Defect type	Without (a)	Thicker struts (b)	Thinner struts (c)	Filled cells (d)	Missing struts (e)
Volume					
Total material volume [mm^3]	141.0	170.4	108.2	144.6	146.0
Total material volume [%]	reference	+20.9	−23.3	+2.6	+3.5
Total defect volume [mm^3]	0.40	0.06	0.08	0.04	0.30
Porosity [%]	0.28	0.04	0.07	0.03	0.21
Outer geometry *(scaling factor of XCT data)*					
Scaling factor in x	0.9925	0.9928	0.9885	0.9948	0.9886
Scaling factor in y	0.9925	0.9928	0.9885	0.9948	0.9886
Scaling factor in z	0.9958	0.9886	0.9836	0.9787	0.9844
Outer geometry *(dimensional variation between measured part and STL file)*					
Dimensional variation in x [%]	0.75	0.72	1.15	0.52	1.14
Dimensional variation in y [%]	0.75	0.72	1.15	0.52	1.14
Dimensional variation in z [%]	0.42	1.14	1.64	2.13	1.56
Overall geometry deviation					
90% < [µm]	117	165	110	142	132
50% < [µm]	53	70	61	69	65
Strut thickness ± SD [mm]	0.595 ±0.010	0.696 ±0.006	0.484 ±0.009	0.597 ±0.008	0.598 ±0.010

5.1. Measurement system

Mass measurements have been performed with a Sartorius balance RC 210 P with a readability of 0.01 mg [5]. The printed and sintered parts were placed individually on the balance at room temperature and without any further pre-treatment like for example drying.

5.2. Measurement protocol

The expected mass (m) of the parts was calculated by the product of final density of the solid material (ρ) and the part volume (V) retrieved from the corresponding STL files:

$$m = \rho^* V$$

Also, the mass was calculated by using the material volume determined by XCT.

By XCT measurement, very few pores are detected in the sintered material. Therefore, it is assumed that the material is almost perfectly dense and the theoretical material density of β-TCP (3.065 g/cm^3 [4]) has been used for further calculation. The calculated values are compared to the measured values, which are represented by a mean of three measurements per part.

5.3. Results

Fig. 6 summarizes the measurement results and shows the mean values of the mass of all parts per defect with standard deviation (±3σ). The expected mass calculated from the volume of the STL data is marked in orange. For all parts, the mass was significantly higher than expected. This deviation comes from a phenomenon called over-polymerization

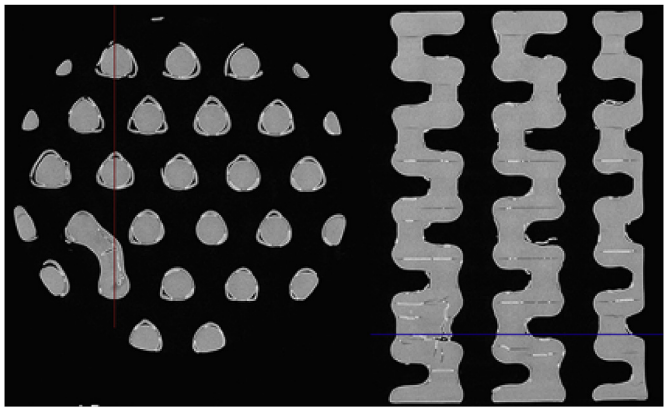

Fig. 5. XCT image of the cylindrical scaffold with missing struts showing also extra material and delamination defects.

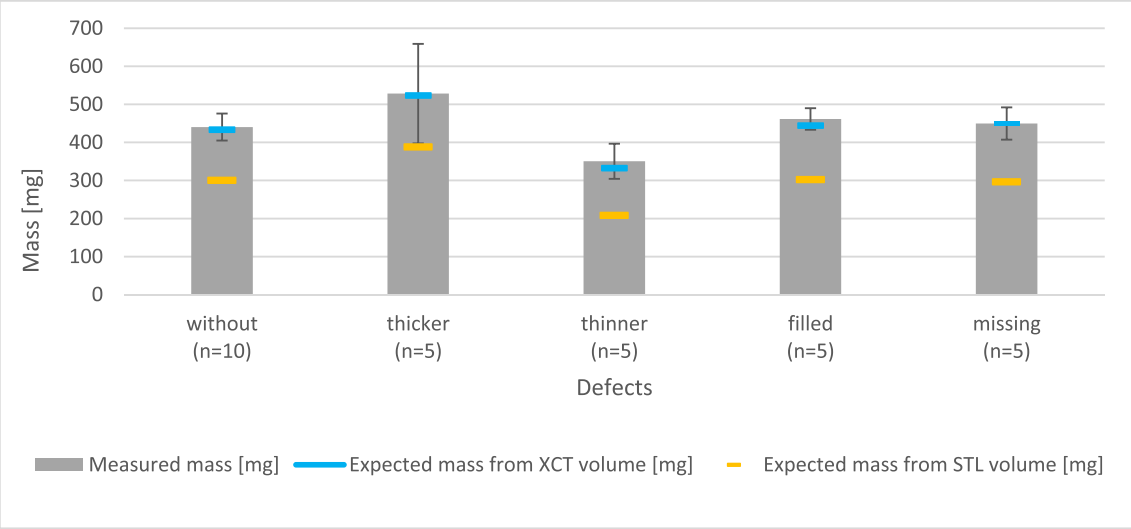

Fig. 6. Mean mass of parts with and without defects with error bars representing the standard deviation (±3σ).

and results from light scattering and refraction during the exposure of the photocurable ceramic suspension. This over-polymerization leads to the curing of areas which are slightly larger than the exposed ones and hence, the resulting struts or walls exhibit higher thicknesses. In principle, such deviations can be compensated using software algorithms but for this study no such measures were taken, which resulted in a significant but uniform deviation from the nominal values of the STL. Insufficient cleaning can also lead to deviations from the nominal mass in dimensions but is not considered as primary cause in the conducted experiments. Due to the low viscosity of the used slurry in LCM, cleaning does not pose any major limitation for channels or pore networks if the diameter is chosen in accordance with the design guidelines and is above a certain threshold, which in the case of interconnected pores as in the printed scaffold is around 200 μm. If cleaning was a major source for deviation from the nominal design there would have been a radial gradient with the highest deviation in the centre and little or no deviations in the regions closer to the outer cylinder jacket. This was not observed in the evaluation of the XCT images.

In case of the part with thinner struts for example, the mass measured corresponds to 160% of the one calculated from the STL volume. In every case, the real part volume is bigger than designed, which was obvious from XCT measurements. In comparison to this, the mass calculated from the volume determined with XCT is indicated using blue marks, which matches the measured mass values.

Whether the means of the sample groups are statistically equal or different in comparison to the reference group without defects was evaluated using the independent two-sample *t*-test (H_0: $\mu = \mu_0$). The tests have been performed at two significance levels at $\alpha = 0.05$ and $\alpha = 0.001$ with 13 degrees of freedom. For $P < \alpha$, the null hypothesis is rejected, which means the difference in mass between the two groups is significant, whereas the mass is assumed to be equal in cases where $P < \alpha$ is not true.

Table 3 allows to conclude, that parts with thicker and thinner struts can be separated from the reference parts by mass, as the difference is significant. No significant difference on the other hand can be stated for the parts with missing struts. The change in the parts mass introduced by this type of defect is minor. The difference in the mass of parts with filled cells is significant compared to the reference at a confidence level of 95% and not significant at a level of 99.9%.

Table 3
Results of independent two-sample *t*-test (H_0: $\mu = \mu_0$) at $\alpha = 0.05$ and $\alpha = 0.001$ for mass measurements.

Tested groups	P	$\mathbf{P < \alpha}$ ($\alpha = 0.05$)	$\mathbf{P < \alpha}$ ($\alpha = 0.001$)
without/thicker	$0.292*10^{-4}$	true	true
without/thinner	$0.144*10^{-7}$	true	true
without/filled	$0.246*10^{-2}$	true	not true
without/missing	0.136	not true	not true

In addition to the mean values presented, the measured values of the single samples are visualized in Fig. 7 (displayed with standard error of the mean of three measurements per part). The range of the mass of the reference parts is marked with two horizontal dotted lines in the diagram below, visualizing the process related variations. From this it is obvious as well, that the mass of the parts with filled cells and the mass of the parts with missing struts are overlapping this range and cannot clearly be distinguished from the parts without defects. Parts with thicker and thinner struts, however, can clearly be separated from parts without defects, except from sample *E5 thicker*. In addition to the designed defect, sample *E5* shows additional defects like broken features from handling and transport, which puts it in the range of the parts without defects and therefore would not have been detected as defect only by weighing.

Lastly, the mass measurements showed that a distinction between parts produced by LCM without defects and thicker or thinner struts, which corresponds to a change in volume and mass of around 20% is possible. The identification of parts with filled cells and missing struts leading to a change in mass of 2.6% respectively 3.5% is not clear, which is related to the variability of the manufacturing process.

6. Defect detection by Archimedes principle

A different fast and easy method to detect variations in the parts manufactured is to determine the volume of the parts by applying the Archimedes principle, which is especially interesting for the volume determination of very complex structures. An object submerged in liquid displaces the liquid in the amount of the object's volume. With the mass of the object in air and the mass of the object submerged, the mass of the displaced liquid is determined and in combination with the density of the liquid, the volume of the object can be calculated [6].

6.1. Measurement system

Measurement of the part's volume was performed with a Sartorius balance RC 210 P with a readability of 0.01 mg [5] in combination with a density determination kit, which allows to measure the mass of the object in air and submerged in a liquid. From both results and the density of the liquid, the parts volume is calculated. To prevent the formation of bubbles in geometrical pores of the parts, the measurements were performed

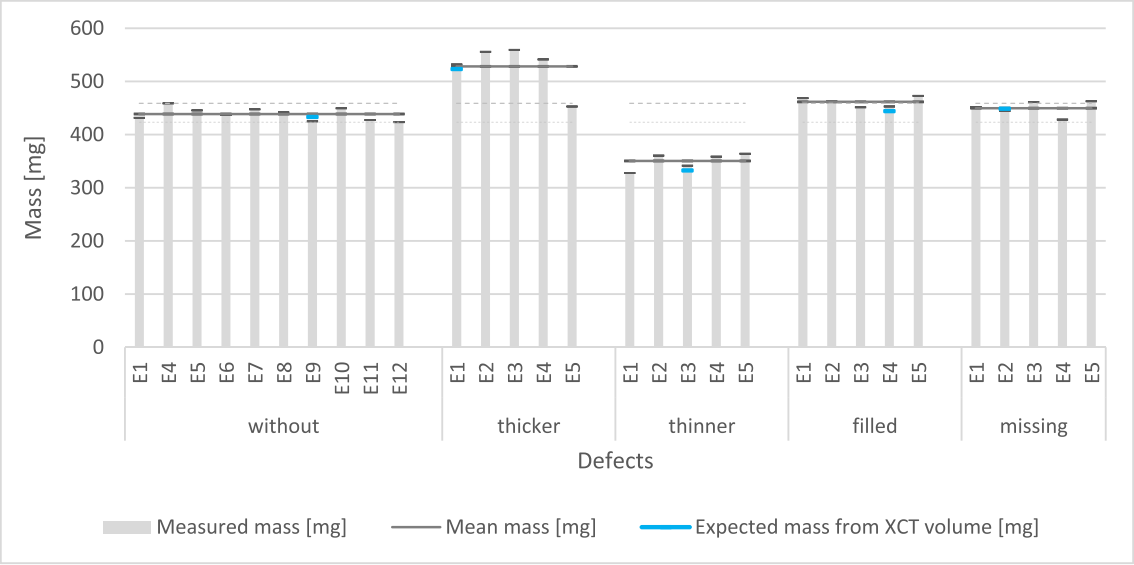

Fig. 7. Mass of parts with and without defects with error bars representing the standard error of the mean ($\sigma/\sqrt{n}$).

in absolute ethanol (min. 99.9%) instead of distilled water due to the reduced surface tension as described in Ref. [7]. The measurements were performed in an air-conditioned room.

6.2. Measurement protocol

The parts were prepared according to the procedure described in international standard ISO 18754 for fine ceramics. In a first step, moisture was removed by drying the parts in a drying chamber over night at 110 °C. Once cooled down to room temperature in a desiccator, the mass of the dry parts was measured. Under vacuum, the parts were covered with absolute ethanol to remove air bubbles. The parts remained for another 30 min in ethanol before the vacuum had been released and measurements of the submerged parts have been performed by placing them in the basket. With the liquid temperature, which was measured at the beginning and at the end of the measurements, the liquid density can be determined.

Using the masses of the dry (m_{dry}) and immersed ($m_{immersed}$) parts and the density of the liquid (ρ_{liquid}), the Volume (V_{part}) of the part can be calculated by:

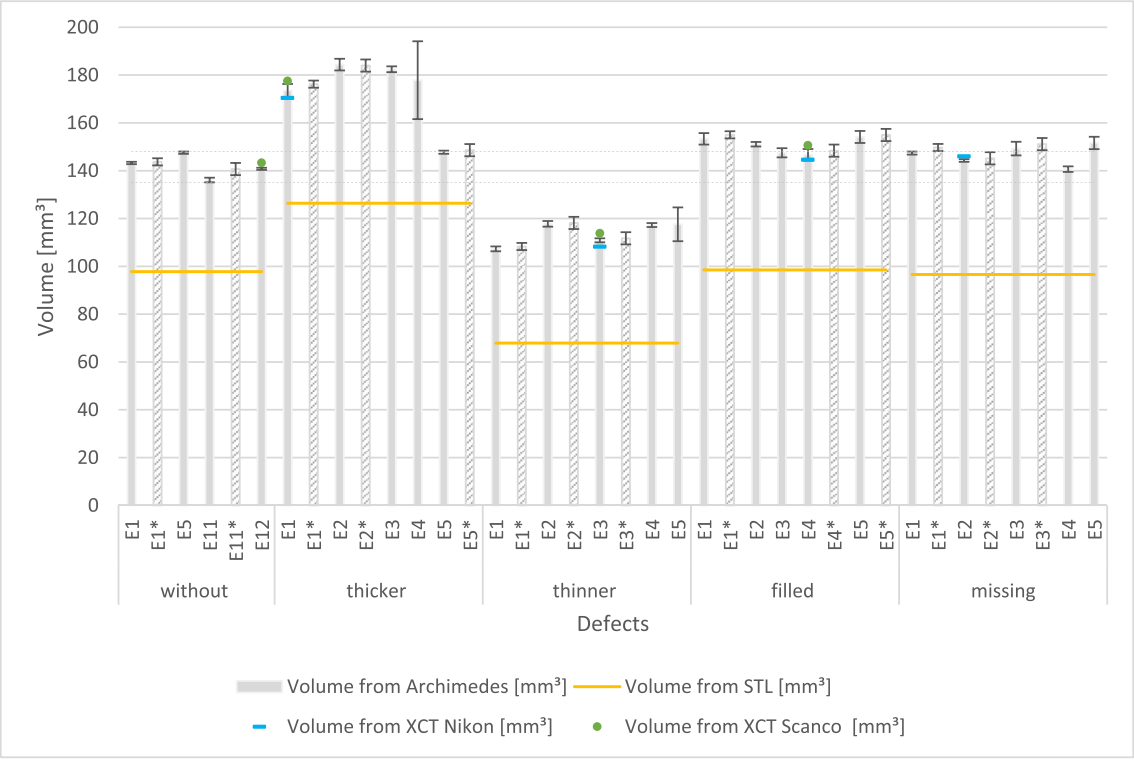

Fig. 8. Volume values of parts with and without defects with error bars representing the combined uncertainty (±3σ).

Table 4
Results of independent two-sample *t*-test (H_0: $\mu = \mu_0$) at $\alpha = 0.05$ and $\alpha = 0.001$ for volume measurements.

Tested groups	P	$\mathbf{P < \alpha}$ ($\alpha = 0.05$)	$\mathbf{P < \alpha}$ ($\alpha = 0.001$)
without/thicker	$0.326*10^{-4}$	true	true
without/thinner	$0.556*10^{-4}$	true	true
without/filled	0.015	true	not true
without/missing	0.162	not true	not true

$$V_{part} = \frac{m_{dry} - m_{immersed}}{\rho_{liquid}}$$

Using the part volume, the geometrical porosity (P) which is the ratio of volume of the free space to the volume of the full cylinder can be calculated by:

$$P = \frac{V_{free\ space}}{V_{full\ cylinder}} = \frac{V_{full\ cylinder} - V_{part}}{V_{full\ cylinder}} * 100$$

The volume of the full cylinder has been determined by measuring height and diameter of each part at three positions with a calliper.

6.3. Results

Four parts without defects have been measured as well as five parts per defect type. The results of volume measurement are visualized in Fig. 8 and displayed with combined uncertainty (±3σ). Some of the parts were measured by two institutes independently. The results from measurements at Laboratoire national de métrologie et d'essais (LNE in Paris, France) are displayed in hatched grey and marked with an asterisk, while measurements at Bundesanstalt für Materialforschung und -prüfung (BAM in Berlin, Germany) are shown in grey. In addition, one part per defect was scanned by XCT and the volume determined for the specific part is marked in blue (part scanned at PTB) and green (part scanned at BAM). The results are in good agreement with the volume measured by Archimedes method. Indicated in orange is once more the expected designed volume from STL data.

An independent two-sample *t*-test (H_0: $\mu = \mu_0$, rejected for $P < \alpha$) performed at two significance levels at $\alpha = 0.05$ and $\alpha = 0.001$ to determine the statistical difference between the means of the sample groups revealed as well significant difference between parts with thicker (not considering sample E5, as it has shown additional ill-defined defects) and thinner struts compared to the reference. Depending on the confidence level required, the difference between parts with filled cells or missing struts is not significant and cannot be safely identified as visible from Table 4.

The geometrical porosity is plotted in Fig. 9, showing that the achieved porosity of the parts is generally lower than expected (orange marks). Again, this deviation can be explained by light scattering and refraction during printing of the parts. While overall dimensional variations are typically lower than 2% in each direction, the variations in volume are much higher. The struts are in every case thicker (approx. 19%) than designed, leading to a reduced geometrical porosity and an increased volume. While the geometrical porosity for the parts without defects, missing struts and filled cells is around 55%, it becomes as expected more porous with thinner struts (approx. 63%) and less porous with thicker struts (approx. 45%). This observation is explicable in terms of the machine parameters leading to the respective geometrical deviations. Sample size and position of struts are determined by the positioning accuracy of the LCM machines mechanical components and the imaging accuracy of the optical system used. This accuracy is overlaid by the saturation, that is, the level of crosslinking of the photo curable feedstock. The influence of an error in saturation and, thus, in voxel size relative to the samples dimensions is small, and almost negligible as the position of struts concerns. On the other hand, the voxel size has a significant impact on the volume of porous structures. Unfortunately, the relation between light exposure and saturation is not linear and depends on various parameters predominately related to the particular feedstock.

To conclude, the Archimedes measurement allows to distinguish defects leading to variations in volume of around 20% in parts produced by LCM. The measurements are in good agreement with the results obtained with XCT measurements. It is of advantage, that using Archimedes principle allows to determine the volume also of complex geometries and with that as well the calculation of overall geometrical porosity, which typically represents a quality attribute for scaffolds intended for bone substitution.

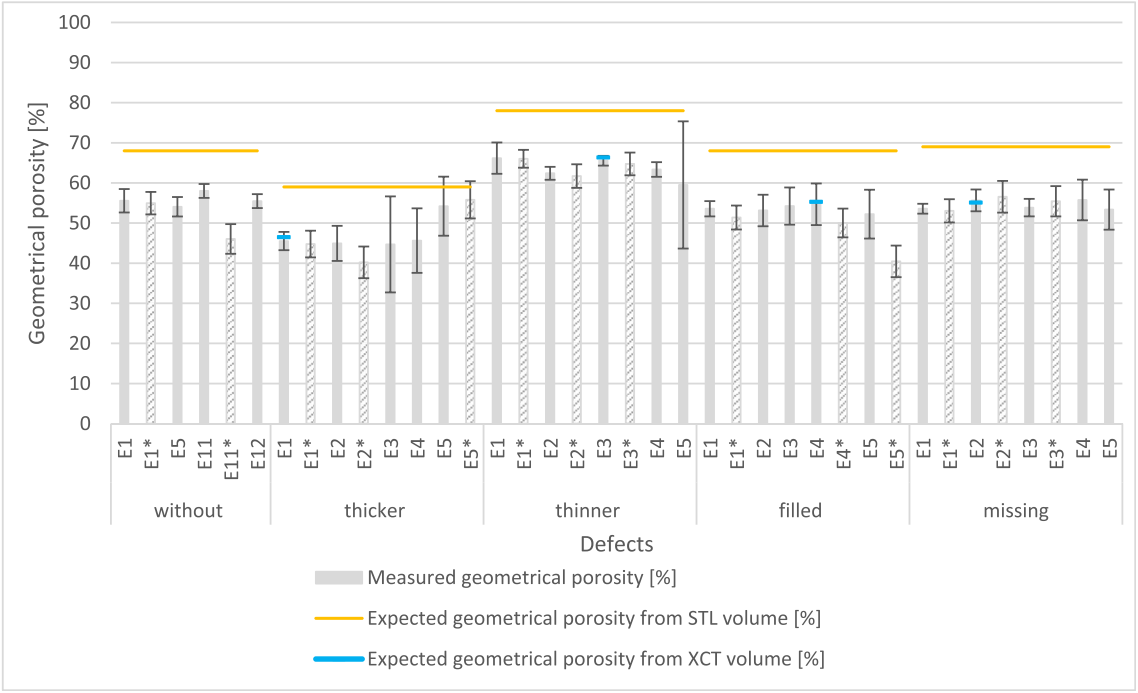

Fig. 9. Geometrical porosity of parts with and without defects with error bars representing the combined uncertainty (±3σ).

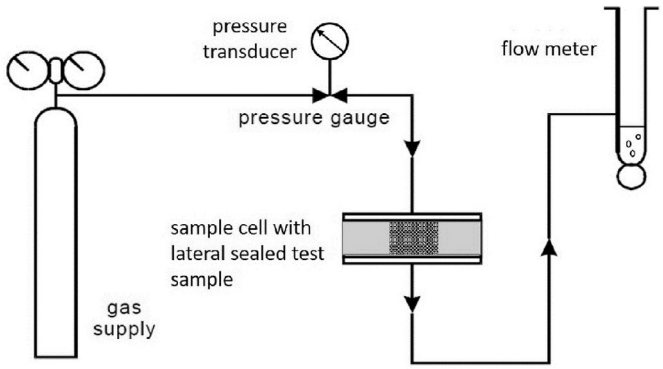

Fig. 10. Schematic test setup of permeability measurement.

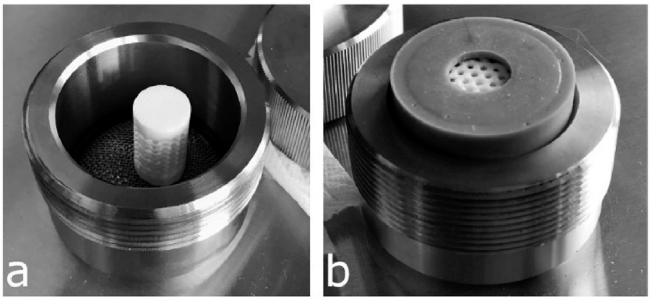

Fig. 11. Measuring cell with sample (a) and sample holder (b).

7. Defect detection by gas permeability

As an approach to detect the minor designed defects in the parts, gas permeability measurements were performed in order to determine whether parts with defects like closed pores can be distinguished from the reference part by means of variations of gas permeability of the ceramic parts.

7.1. Measurement system

The capillary flow porometer Porolux 1000 (IB-FT GmbH) allows the measurement of gas permeability of porous materials. During the measurement, an inert gas flows vertically through the porous sample at default pressure and at constant temperature. The test runs with an elevated inlet pressure relative to the outlet pressure that is kept at atmospheric pressure. The gas flow is measured as a function of time at constant pressure. To ensure that the gas flows only in vertical direction through the sample, the lateral surface of the sample must be tightly sealed. A schematic test setup of a permeability measurement is shown in Fig. 10.

The porometer set-up has been actually planned for the analysis of mineral building materials, such as cementitious mortars and natural stones. They are characterized by much smaller mesopores and capillary pores than the broader and interconnected pores coming from the design of the ceramic parts. Thus, the porometer contains three volumetric gas flow meters with 30 ml/min, 1 l/min and 20 l/min, which automatically adjust to the current measuring range, and two pressure transducers with automatic switch-over.

7.2. Measurement protocol

The smallest measuring cell with diameter/height ratio of 25/10 mm was used. Prior to the measurement, a sample holder, which completely fills the measurement cell and tightly seals the lateral sample surface must be built. Therefore, a mould in the size of the measuring cell was fabricated and filled with additive-curing silicone duplicating compound *Deguform® plus* from *DeguDent*. The measurement cell with a cylindrical sample is shown in Fig. 11a without sample holder and in Fig. 11b with sample holder.

Prior to a permeability measurement, diameter and thickness of the sample were measured. Afterwards, the dry and sealed sample was put in the measuring cell. The permeability measurements were carried out with nitrogen at 20 °C. Relative inlet pressures between 1 and 2 kPa were used. At default pressure, the gas flow rate needs to reach steady-state conditions, which was usually achieved within 2–10 min. At that point, the volume flow rate of the gas was measured. The measurement was repeated several times while the default pressure was changed slightly to verify that the gas flow is laminar.

The underlying principle is the Hagen-Poiseuille relationship for laminar flow of a compressible fluid through a porous solid with small capillaries under steady-state conditions. The relationship solved for the specific gas permeability coefficient K [m^2] can be written as:

$$K = \eta * \frac{Q^* L}{A} * \frac{2p}{(p_e - p_a) * (p_e + p_a)}$$

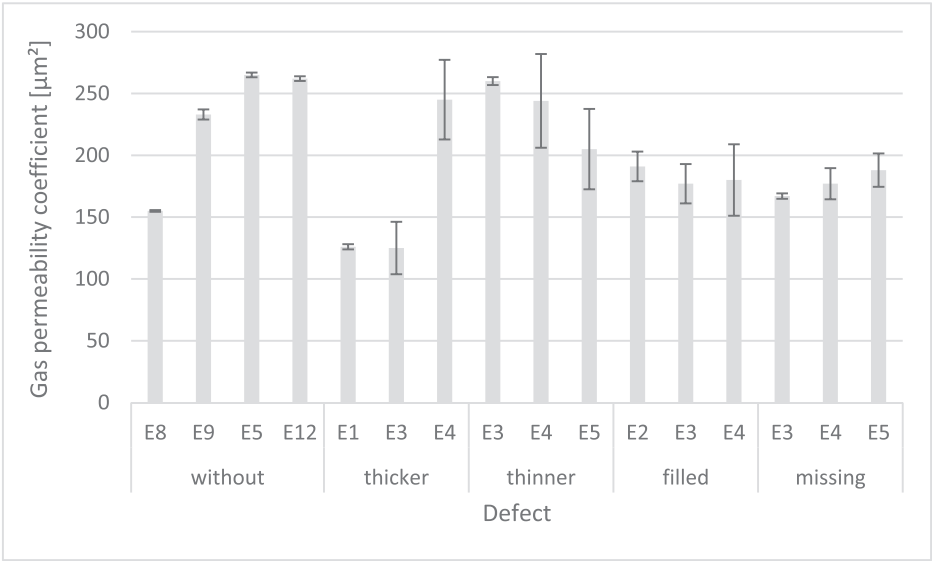

Fig. 12. Gas permeability coefficient of parts with and without defects with error bars representing the standard deviation (±1σ).

with the gas viscosity $\eta(1.74 \cdot 10^{-5}$ N/m^2 for nitrogen at 20 °C), the measured volume flow rate Q in m^3/s, the sample thickness parallel to the flow direction L in m, the cross-section area of the sample A in m^2, the default absolute pressure $p$in N/m^2, at which the volume flow rate is measured, the absolute gas inlet pressure p_e in N/m^2 and the absolute gas outlet pressure p_a in N/m^2. [8,9]

7.3. Results

On four parts without defects and three parts for each defect, the volume flow rate was measured at default pressure and the gas permeability coefficient was calculated. Fig. 12 shows the results together with the scattering of the data points. The permeability coefficients of all TCP scaffolds range between $1.0*10^{-10}$ and $2.5*10^{-10}$ m^2, which are entirely typical values for porous ceramic foams [10]. But the results do not allow to safely differentiate between parts with or without defects.

The gas permeability coefficient of the samples, especially in the category without defects or with thicker struts, vary randomly and do not enable reliable conclusion regarding included defects. Only two of three parts with thicker struts appear to show lower permeability coefficients as expected. Possible reasons for the random variation of results might arise from the microstructure of TCP parts itself as well as the test set-up of the measuring instrument. The changes in the parts by the defects are tiny in relation to the flow-through volume of the coarse pores. Furthermore, the designed pores in the parts might deviate from the assumption of uniform cylindrical pores with smooth pore walls. Thus, the nitrogen flow through the parts could differ from the required laminar conditions leading to random results. The used pressure transducer of the instrument could be inconvenient for these samples with coarse pores because the default pressure applied is near the lower limit of the measuring range. Further parameter studies and a more adequate instrument set-up might lead to more reliable results.

8. Conclusion

In conclusion, the results in this article show that both weighing and Archimedes measurement to determine the volume are simple, cost-effective methods for quality control within the manufacturing chain of additively manufactured porous structures. For the parts produced by LCM both approaches allowed to distinguish between parts without defects and parts with defects leading to changes in mass and volume of 20% and more. Detection of minor defects is limited due to process related variations in the parts geometry.

In addition, Archimedes measurements allow to control the geometrical porosity of lattice parts, which is considered as quality attribute for lattice medical implants.

Defect detection with the gas permeability instrument used here was not successful. No significant changes in flow rates could be detected for the studied defect types. Nevertheless, the measuring principle appears promising due to its simple measurement protocol. The method can be developed further with an optimized instrument set-up, such as pressure transducer and flow meter for smaller measuring ranges as well as smaller measuring cells.

Attention should also be payed to the conversion step from CAD to STL file format, when thinking of error sources along the additive manufacturing process chain. The deviations observed in this case due to the conversion led to a volume change of about 2%.

Funding

The work was supported by the project “MetAMMI” (15 HLT09) and has received funding from the EMPIR programme co-financed by the Participating States and from the European Union’s Horizon 2020 research and innovation programme.

Declaration of competing interest

M.S. is an employee of the company Lithoz GmbH, supplier of the used LithaBone suspension and the CeraFab 3D printer. The author declares no competing interests.

References

[1] EMPIR Project- JRP Protocol – Annex I v, 2, Metrology for Additively Manufactured Medical Implants (15HLT09 MetAMMI), 2016.
[2] Lithoz GmbH, Die LCM-Technologie von Lithoz, accessed, http://www.lithoz.com/additive-manufacturing/lcm-verfahren, 2017. (Accessed 23 September 2018).
[3] R. Felzmann S. Gruber, G. Mitteramskogler, P. Tesavibul, A.R. Boccaccini, R. Liska, J. Stampfl, Lithography-based additive manufacturing of cellular ceramic structures, Adv. Eng. Mater. 14 (2012) 1052–1058.
[4] Lithoz GmbH, LCM technology – material overview - technical data LithaBone TCP 300, accessed, https://www.lithoz.com/application/files/2315/5197/6789/2019_1_Materialfolder_EN_Print-1.pdf, 2019. (Accessed 14 October 2019).
[5] Sartorius AG: Sartorius Research Series – Product Data Sheet – MC1, WRC 6002-e93042.
[6] Sartorius AG:, YDK 01, YDK 01-0D, YDK 01LP Density Determination Kit, Manual (98647-002-37).
[7] A.-F. Obaton, M.-Q. Lê, V. Prezza, D. Marlot, P. Delvart, A. Huskic, S. Senck, E. Mahé, C. Cayron, Investigation of new volumetric non-destructive techniques to characterize additive manufacturing parts, Weld. World 62 (2018) 1049–1057.
[8] H. Gräf, H. Grube, Verfahren zur Prüfung der Durchlässigkeit von Mörteln und Beton gegenüber Gasen und Wasser, Beton 36 (1986) 184–187.
[9] J.J. Kollek, The determination of the permeability of concrete to oxygen by the Cembureau method - a recommendation, Mater. Struct. 22 (1989) 225–230.
[10] J. R Zeschky, Keramikschäume aus gefüllten Polysilsesquioxanen, Dissertation, University Erlangen-Nürnberg, 2004.